ACS chemical biology

Articles

Cite This: ACS Chem. Biol. 2019, 14, 674−687

pubs.acs.org/acschemicalbiology

Fimsbactin and Acinetobactin Compete for the Periplasmic Siderophore Binding Protein BauB in Pathogenic *Acinetobacter baumannii*

Tabbetha J. Bohac, Luting Fang, Daryl E. Giblin, and Timothy A. Wencewicz*

Department of Chemistry, Washington University in St. Louis, One Brookings Drive, St. Louis, Missouri 63130, United States

Supporting Information

ABSTRACT: Environmental and pathogenic microbes produce siderophores as small iron-binding molecules to scavenge iron from natural environments. It is common for microbes to produce multiple siderophores to gain a competitive edge in mixed microbial environments. Strains of human pathogenic *Acinetobacter baumannii* produce up to three siderophores: acinetobactin, baumannoferrin, and fimsbactin. Production of acinetobactin and baumannoferrin is highly conserved among clinical isolates while fimsbactin production appears to be less common. Fimsbactin is structurally related to acinetobactin through the presence of catecholate and phenolate oxazoline metal-binding motifs, and both are derived from nonribosomal peptide assembly lines with similar catalytic domain orientations and identities. Here we report on the chemical, biochemical, and microbiological investigation of fimsbactin and acinetobactin alone and in combination. We show that fimsbactin forms a 1:1 complex with iron(III) that is thermodynamically more stable than the 2:1 acinetobactin ferric complex. Alone, both acinetobactin and fimsbactin stimulate *A. baumannii* growth, but in combination the two siderophores appear to compete and collectively inhibit bacterial growth. We show that fimsbactin directly competes with acinetobactin for binding the periplasmic siderophore-binding protein BauB suggesting a possible biochemical mechanism for the phenomenon where the buildup of apo-siderophores in the periplasm leads to iron starvation. We propose an updated model for siderophore utilization and competition in *A. baumannii* that frames the molecular, biochemical, and cellular interplay of multiple iron acquisition systems in a multidrug resistant Gram-negative human pathogen.

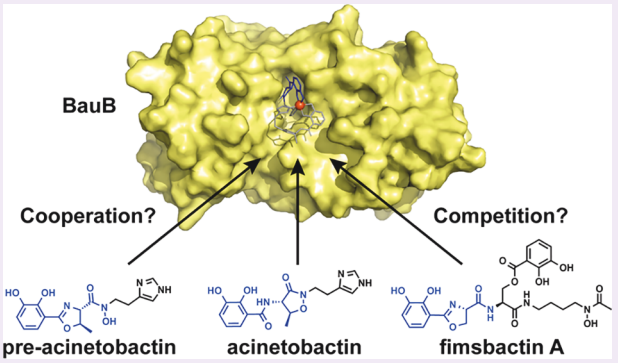

The rise of infections caused by multidrug resistant (MDR) Gram-negative pathogens, including MDR *Acinetobacter baumannii*, is driving the exploration of nontraditional therapeutic strategies including antivirulence therapies.[1,2] Blocking virulence pathways such as cellular adhesion, protein secretion, biofilm formation, motility, and nutrient acquisition are presumed to apply less selective pressure for resistance and might work synergistically with traditional antibiotics.[3] Targeting nutrient acquisition pathways is an attractive option since a disproportionate percentage of the pathogen's conditionally essential genome is comprised of genes associated with nutrient scavenging.[4,5] However, concern over the presence of multiple, seemingly redundant pathways has raised concern as to whether inhibiting one nutrient scavenging pathway is enough to slow pathogen growth *in vivo*.[6] For example, pathogenic strains of *A. baumannii* express several types of protein machinery that contribute to iron acquisition including dedicated pathways for the transport of ferrous (*feoABC*),[7,8] heme (*hemO* and *hemT* gene clusters),[9] and siderophore (*basA*−*J*, *bauA*−*F*, *barAB*, *fbsA*−*Q*, *bfnA*−*L*, *fhuE*, *piuA*, *pirA*, *tonB*, and *exbBD*)[10−14] iron sources.[15] It remains to be determined if blocking one of these iron acquisition pathways alone will be effective *in vivo* as an antivirulence approach. A more comprehensive understanding of the interplay and conditional dependence between the available iron scavenging pathways is needed to determine the best approach for developing effective antivirulence agents that disrupt said pathways.

At least three unique structural families of siderophores (acinetobactin,[16] fimsbactin,[11] and baumannoferrin/acinetoferrin[12,17]) have been detected from clinical isolates of *A. baumannii* and *A. hemolyticus* (Figure 1a). Acinetobactin (Acb) is the most studied *A. baumannii* siderophore and is highly conserved in all clinical isolates.[15] Acinetobactin is produced via a nonribosomal peptide synthetase (NRPS) biosynthetic assembly line (Supplementary Figure 1).[18,19] Preacinetobactin is the kinetic product released from the NRPS, and Acb is the thermodynamic product resulting from spontaneous isomerization of PreAcb.[20] Both PreAcb and Acb form stable 2:1 ferric complexes, [Fe(PreAcb)$_2$] and [Fe(Acb)$_2$], respectively, and stimulate *A. baumannii* growth under iron limiting conditions.[21,22] Isomerization of PreAcb is slow under acidic

Received: December 3, 2018
Accepted: February 20, 2019
Published: February 20, 2019

DOI: 10.1021/acschembio.8b01051
ACS Chem. Biol. 2019, 14, 674−687

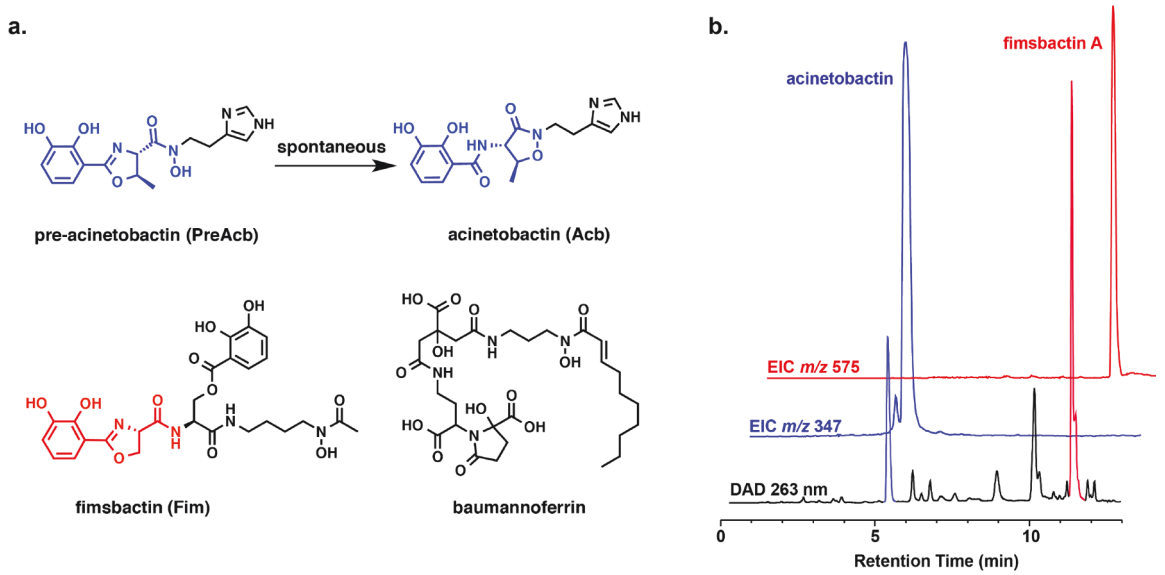

Figure 1. Siderophores from *A. baumannii*. (a) Structures of preacinetobactin (PreAcb), acinetobactin (Acb), fimsbactin (Fim), and baumannoferrin. PreAcb/Acb and Fim share a common motif derived from condensation of 2,3-DHB with L-Thr (PreAcb/Acb) or L-Ser (Fim). (b) DAD at 263 nm (black), EIC at *m/z* 347 (blue), and EIC at *m/z* 575 (red) chromatograms from LC-MS analysis of crude *A. baumannii* ATCC 17978 supernatant after acidification, treatment with XAD-7HP resin, and methanol elution. Baumannoferrin was not detected.

conditions ($t_{1/2} \approx 16$ h, pH 5.5), and chelation of iron(III) prevents isomerization, which has led to speculation that both PreAcb and Acb have a natural role in iron scavenging under acidic infection conditions.[20]

The fimsbactin siderophores, fimsbactin A−F, were discovered in 2013 and are also derived from an NRPS assembly line resembling the Acb NRPS system (Supplementary Figure 1).[11,23] Fimsbactin A (Fim) was the primary siderophore in the mixture isolated from *A. baylyi* ADP1 accounting for >85% of the total mass (Figure 1a). The remaining fimsbactin metabolites, B−F, appear to be shunt biosynthetic products, biosynthetic intermediates, or analogs resulting from the incorporation of L-Thr instead of L-Ser into the siderophore backbone (Supplementary Figure 2). PreAcb/Acb and Fim are structurally related by the catecholate, phenolate oxazoline, and hydroxamate metal-binding motifs found in common siderophores such as enterobactin,[24] vibriobactin,[25] and heterobactin,[26] respectively.

Baumannoferrin is the most recently characterized *A. baumannii* siderophore, discovery of which was reported in 2015, and is derived from an NRPS-independent siderophore synthetase (NIS) biosynthetic process.[12] A related NIS siderophore, acinetoferrin, has been reported from environmental strains and the opportunistic human pathogen *Acinetobacter haemolyticus*.[17,27] Baumannoferrin is structurally distinct from the NRPS siderophores PreAcb, Acb, and Fim. The structure is composed of citrate, 1,3-diaminopropane, 2,4-diaminobutyrate, decenoic acid, and α-ketoglutarate.[12] The lipophilic nature of the baumannoferrin decenoic acid side chain has led to the proposal that the siderophore might be membrane associated.[28] The structure contains one hydroxamate and two α-hydroxy carboxylate metal-binding motifs similar to chelating groups found in other NIS-derived citrate-based siderophores such as aerobactin produced by human pathogens including *Klebsiella pneumonia* and uropathogenic *E. coli* (UPEC).[29,30]

Biosynthetic operons (Supplementary Figure 3) for baumannoferrin and PreAcb/Acb are present in all genome-sequenced clinical isolates of *A. baumannii* deposited in the NCBI database (taxid: 470).[15] In contrast, only 4 unique strains (<10% of sequenced *A. baumannii* strains) contain genes associated with fimsbactin biosynthesis and utilization (Supplementary Figure 4). It appears as though human pathogenic strains of *A. baumannii* always retain the capacity for producing at least two siderophores, PreAcb/Acb and baumannoferrin, or occasionally three siderophores if the Fim biosynthetic operon is present and functional. Since Fim production is optional for pathogenicity, this raises the question as to whether the structural similarity of PreAcb/Acb and Fim is functionally redundant or if the siderophore pathways contribute cooperatively to the acquisition of iron and other metal ions leading to increased pathogen virulence.

It is common for pathogenic and environmental microbes to produce multiple siderophores either via the presence of multiple biosynthetic gene clusters (as for PreAcb/Acb, Fim, and baumannoferrin in *A. baumannii*), production of shunt/fragment biosynthetic products (as for fimsbactin A−F), precursor-directed biosynthesis (as for fimsbactin incorporation of Thr or Ser), or biosynthetic tailoring reactions (as for acyl-enterobactins[31]).[32] Additionally, pathogens often produce siderophore transport proteins for siderophores produced by neighboring bacteria, so-called xenosiderophores.[33] Pathogenic *A. baumannii* express the protein FhuD to enable the utilization of hydroxamate-based xenosiderophores including desferrioxamine B.[13] Potential advantages of utilizing multiple siderophores[32,34] include synergistic effects of siderophore combinations on iron acquisition,[20] evasion of immune proteins such as siderocalin,[35] suppression of competing microbial growth,[36,37] stimulation of cooperative and synergistic microbial growth,[38,39] expansion of metal uptake beyond iron,[40,41] quorum sensing and cell signaling,[42] nutritional passivation of necessary but potentially toxic metals,[43,44] quenching of reactive oxygen species,[45,46] and induction of metal-dependent cellular responses in the host.[47,48]

We sought to investigate the interplay of two high-affinity *A. baumannii* siderophore-based iron acquisition systems, the

DOI: 10.1021/acschembio.8b01051
ACS Chem. Biol. 2019, 14, 674−687

PreAcb/Acb and Fim pathways. Prior to this work, there were no reports on the metal chelating properties of Fim, and growth promotion of *A. baumannii* by Fim had not been demonstrated. Here, we show that Acb or Fim alone stimulates *A. baumannii* growth under iron-deficient conditions. Both siderophores promote growth more efficiently in the holo, iron-bound forms. Surprisingly, we found that apo-Fim is antagonistic toward holo-Acb leading us to hypothesize that Acb and Fim have competing utilization pathways. We recently reported the X-ray crystal structure of the periplasmic siderophore-binding protein BauB bound to a stable $[Fe(Acb)_2]^-$ ferric complex, which provided a template for understanding siderophore molecular recognition in *A. baumannii*.[21] In this work, we show that both isomers of acinetobactin, PreAcb and Acb, and Fim bind to BauB with nanomolar affinity. Intrinsic fluorescence quenching and direct binding via an immobilized BauB-LC-MS competition experiment validated a meaningful binding interaction between BauB and the apo- and holo-forms of PreAcb, Acb, and Fim. The substrate binding promiscuity of BauB is explained using density functional theory (DFT) calculated structures of the $[Fe(PreAcb)_2]^-$ and $[Fe(Fim)]^-$ complexes compared to the BauB·$[Fe(Acb)_2]^-$ crystal structure. Structure comparison reveals how the three *A. baumannii* siderophores fulfill the octahedral iron(III) coordination sphere using ligands derived from the common 2,3-DHB-Thr/Ser phenolate oxazoline, catechol, and imidazole/hydroxamate motifs. All three ferric complexes share identical stereochemistry about the ferric metal center with clear overlapping of electron density in the ligand-to-metal coordination sphere. Pathway competition between Acb and Fim might explain in part why it is rare to find clinical isolates of pathogenic *A. baumannii* harboring biosynthetic operons for both siderophores.

RESULTS AND DISCUSSION

Purification of Acb and Fim from *A. baumannii* ATCC 17978. The fimsbactin siderophores were originally isolated from the environmental strain *A. baylyi* ADP1.[11] Up to this point, Fim had not been isolated from any pathogenic strains of *A. baumannii* although comparative genomics predicts the presence of the Fim operon in at least 4 unique strains of *A. baumannii* in the NCBI database (Supplementary Figure 4). One of these strains is human pathogenic *A. baumannii* ATCC 17978, a clinical isolate that is predicted to be a producer of Acb, Fim, and baumannoferrin.[49] We isolated crude Acb and fimsbactin A–F from *A. baumannii* ATCC 17978 grown in iron-deficient M9 minimal medium at 37 °C. LC-MS analysis of the crude fermentation broths from two separate trials showed the presence of Acb and all of the fimsbactin isomers, fimsbactin A–F, with fimsbactin A providing the largest signal in the optical absorbance and extracted ion chromatogram (EIC) traces (Figure 1b; Supplementary Figures 5, 6). This validates coproduction of Acb and Fim by a human pathogenic strain of *A. baumannii*. Acb and fimsbactin A were purified via RP-C18 prep-HPLC allowing for isolation of both siderophores from a single fermentation. Acb was isolated in >95% purity by LC-MS at a mass recovery after purification of 31 mg/L averaged over two trials (Supplementary Figure 7). No PreAcb was observed, which is consistent with the instability of PreAcb during extended fermentations at physiological pH and previous failed isolation attempts. However, PreAcb is readily available in our group through total synthesis.[20] Fimsbactin A, hereon referred to as Fim, was isolated as a mixture of fimsbactin A (>90%) and fimsbactins B, C, and F (≤10%) according to LC-MS and NMR analysis. We validated that fimsbactin A is the primary component by HRMS and comparison of the 1D (^{1}H, ^{13}C) NMR spectra against the literature reported values (Supplementary Table 1; Supplementary Figures 8–12).[11] The mass recovery of Fim after purification was 5 mg/L averaged over two independent trials. The greater mass production of Acb over Fim is consistent with the observations for siderophore production in *A. baylyi*.[11] We were unable to detect any positively charged ions corresponding to apo- or holo-baumannoferrin in the *A. baumannii* ATCC 17978 supernatants despite the predicted biosynthetic capacity for this siderophore (Supplementary Figure 4).[12] It is possible that the baumannoferrins remain membrane associated or have a low ionization potential in positive mode electrospray ionization (ESI), due to the anionic carboxylate/hydroxamate metal-chelating groups, thus proving to be undetectable by the low-resolution single quadrupole mass spectrometer employed in this study.[50] We utilized synthetic PreAcb, natural Acb, and natural Fim (>90% fimsbactin A) for all studies in this work.

Iron-Binding Properties of Fim. Fim is a mixed ligand biscatecholate-monohydroxamate siderophore that is structurally related to other NRPS siderophores including heterobactin[26] and vibriobactin[25] (Figure 2; Supplementary Figure 13). These related siderophores are hexadentate metal chelators with three bidentate ligands (either catecholates, phenolate oxazolines, or hydroxamates) branching from three arms of a tetrahedral atom, either nitrogen or carbon, creating a tripodal ferric coordination template. Vibriobactin is spermidine-based with a tetrahedral nitrogen at the apex of the tripod, while Fim and heterobactin are amino acid-based

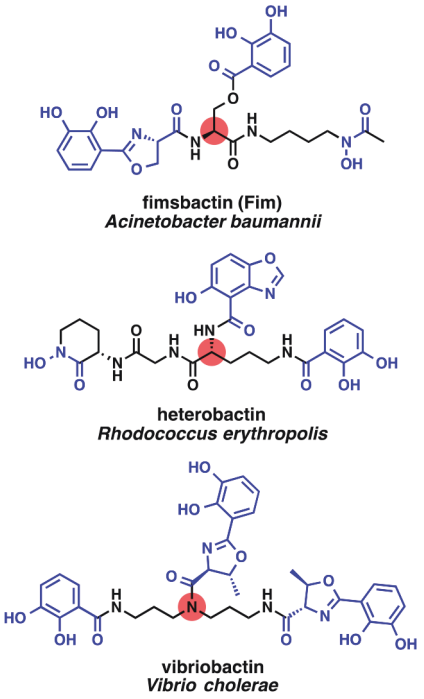

Figure 2. Structures of Fim (*A. baumannii*), heterobactin (*Rhodococcus erythropolis*), and vibriobactin (*Vibrio cholerae*) siderophores. Metal chelating groups are shown in blue. The tetrahedral atom is highlighted by a salmon sphere.

DOI: 10.1021/acschembio.8b01051
ACS Chem. Biol. 2019, 14, 674–687

Table 1. Siderophore Iron Binding Properties and Apparent BauB Dissociation Constants (K_d)

siderophore	siderophore/Fe(III) stoichiometry[a]	metal/ligand charge transfer band (λ_{abs}, nm)	apparent logK_{Fe}[b]	apparent BauB K_d (nM)[c]
PreAcb	2:1	515	27.4 ± 0.2	380 ± 110 (750 ± 160)
Acb	2:1	570	26.2 ± 0.1	300 ± 100 (160 ± 80)
Fim	1:1	445	27.1 ± 0.2	360 ± 140 (240 ± 90)

[a]Siderophore/Fe stoichiometry was measured by titration of siderophores with $Fe(acac)_3$ monitored by quenching of intrinsic siderophore fluorescence. [b]Apparent log K_{Fe} values for $[Fe(PreAcb)_2]$ and $[Fe(Acb)_2]$ are literature values.[20] [c]Values in parentheses are for the ferric holo-siderophore complexes. The apparent K_d for Acb and $[Fe(Acb)_2]$ are literature values.[21] Data is reported as mean ± standard deviation from the mean for at least two independent trials.

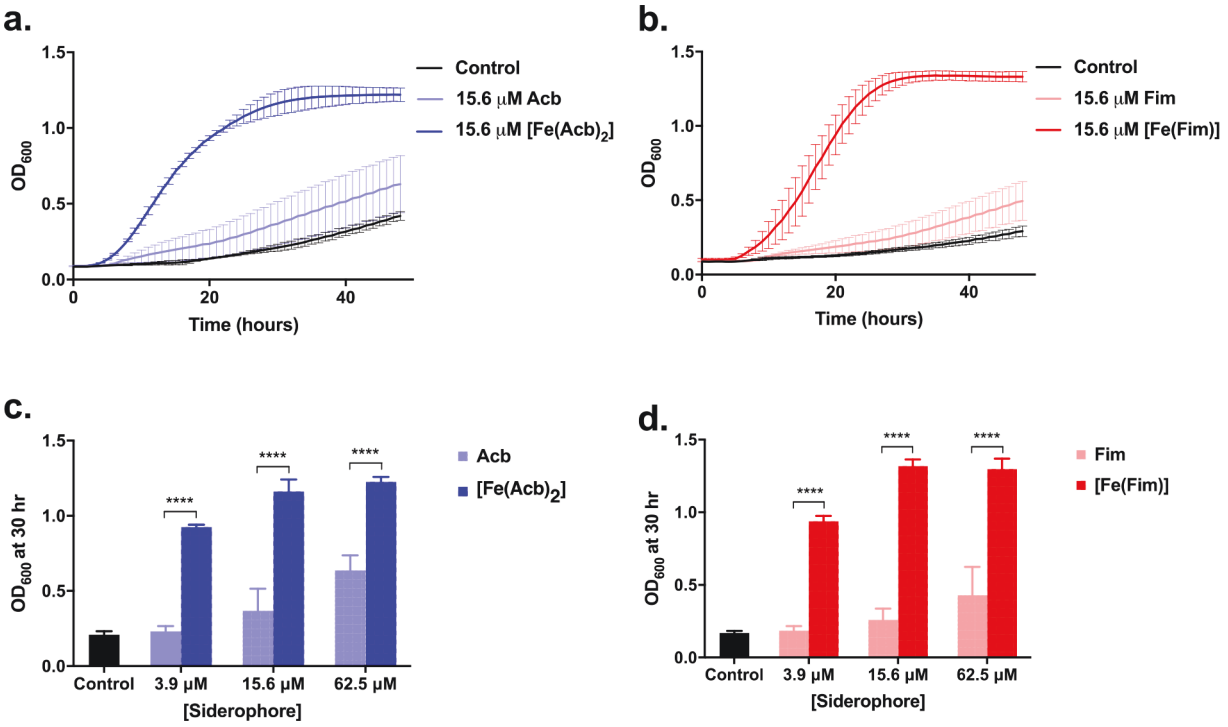

Figure 3. Influence of apo- and holo-siderophores on *A. baumannii* growth. Line graphs depict the growth of *A. baumannii* ATCC 17978 determined by measuring the optical density at 600 nm (OD_{600}) at 37 °C as a function of time in the presence of (a) Acb or $[Fe(Acb)_2]$ and (b) Fim or [Fe(Fim)]. Bar graphs depict the comparison of OD_{600} values after 30 h in the presence of variable concentrations of (c) Acb or $[Fe(Acb)_2]$ and (d) Fim or [Fe(Fim)]. Error bars represent standard deviations from the mean for three independent trials, ****$p < 0.0001$.

using the α-carbon of L-Ser or L-Lys, respectively, as the tetrahedral branch point for the three metal-chelating ligands.

Fim is composed of hydroxamate, phenolate oxazoline, and catecholate metal-chelating groups derived from *N*-acetyl-*N*-hydroxy-cadaverine, serine-2,3-DHB oxazoline, and 2,3-DHB, respectively.[11] Heterobactin contains hydroxamate, phenolate oxazoline, and catecholate ligands derived from cyclized *N*-hydroxy-ornithine, 2,5-dihydroxy-6-amino-benzoate, and 2,3-DHB, respectively.[26] Heterobactin forms a stable 1:1 ferric complex with a ligand-to-metal charge transfer band in the optical absorbance spectra appearing at 520 nm.[51] For comparison, the well-known 1:1 enterobactin tris-catecholate ferric complex has a characteristic ligand-to-metal charge transfer band at 498 nm.[52] We sought to investigate the iron binding properties of Fim in comparison to PreAcb and Acb to better understand metal chelation dynamics of the mixed siderophore system in *A. baumannii*.

Ferric complexes of PreAcb, Acb, and Fim were prepared by treatment with $Fe(acac)_3$ using a method reported previously by our group.[20,22,33,53] Titration of Fim with $Fe(acac)_3$ or $FeCl_3$ in MeOH monitored by fluorescence quenching ($\lambda_{excitation}$ = 330 nm; $\lambda_{emission}$ = 380 nm) was consistent with the formation of a stable [Fe(Fim)] ferric complex (Supplementary Figure 14). At 0.5 equiv of Fe(III), the titration curve indicates formation of 2:1 $[Fe(Fim)_2]$ complex that converts to a 1:1 [Fe(Fim)] complex once stoichiometric Fe(III) is added. These observations are consistent with previous studies of mixed ligand siderophores, including heterobactin, where ligand-to-metal stoichiometry of ferric complexes varied with metal/ligand concentrations and pH.[51] LC-MS analysis of [Fe(Fim)] produced an $[M + H]^+$ ion with an observed m/z = 627 consistent 1:1 siderophore/iron(III) stoichiometry. Both PreAcb and Acb form 2:1 siderophore/iron complexes, $[Fe(PreAcb)_2]$ and $[Fe(Acb)_2]$, respectively, that lose iron upon ionization by ESI in positive ion mode to give $[M + H]^+$ ions with m/z 347 corresponding to the expected mass of apo-Acb.[20,21] This difference in ionization modes reflects the increased relative stability of a 1:1 siderophore/iron complex, [Fe(Fim)], compared to 2:1 siderophore/iron complexes, $[Fe(PreAcb)_2]$ and $[Fe(Acb)_2]$, toward ESI. The optical absorbance spectrum of [Fe(Fim)] shows a broad ligand-to-metal charge transfer absorbance band at 445 nm (Supplementary Figure 15). $[Fe(PreAcb)_2]$ and $[Fe(Acb)_2]$ show ligand-to-metal charge transfer absorbance

DOI: 10.1021/acschembio.8b01051
ACS Chem. Biol. 2019, 14, 674−687

bands at 515 and 570 nm, respectively, in the optical absorbance spectra.[20] The red spectral shift for [Fe(Fim)] (λ_{max} = 445 nm) compared to [Fe(PreAcb)$_2$] (λ_{max} = 515 nm) and [Fe(Acb)$_2$] (λ_{max} = 570 nm) implies that there are greater interactions between ferric iron and stronger-field ligands in the [Fe(Fim)] complex.[52]

We measured the apparent Fe(III) affinity (log K_{Fe}) of [Fe(Fim)] to be 27.1 ± 0.2 using an EDTA competition assay (Table 1; Supplementary Figure 16). The apparent stability of the [Fe(Fim)] ferric complex is similar to [Fe(PreAcb)$_2$] (apparent log K_{Fe} = 27.4 ± 0.2) and greater than [Fe(Acb)$_2$] (apparent log K_{Fe} = 26.2 ± 0.1).[20] We confirmed that apparent K_{Fe} for FimFe was greater than Acb$_2$Fe through a competitive iron exchange assay. Treatment of [Fe(Acb)$_2$] with an equimolar amount of apo-Fim resulted in formation of the [Fe(Fim)] complex as confirmed by optical absorbance spectroscopy (Supplementary Figure 17). The metal exchange was slow, as expected, and complete conversion was achieved after 20 h suggesting that the 1:1 [Fe(Fim)] ferric complex is thermodynamically more stable than the 2:1 [Fe(Acb)$_2$) complex. The relevance of iron exchange between siderophores is unknown, but it could play a role in the overall iron acquisition process through a metal shuttle.[54] Similar differences in ferric complex stability of siderophores have been reported for mycobactin (more stable; phenolate oxazoline, bis-hydroxamate) and exochelin (less stable; imidazole-containing bis-hydroxamate) from *Mycobacterium tuberculosis*.[55] We sought to investigate the potential for siderophore cooperativity between combinations of Fim, PreAcb/Acb, and the corresponding ferric complexes by performing *A. baumannii* growth promotion studies.

Fimsbactin A Stimulates *A. baumannii* Growth under Iron-Deficient Conditions. Formation of stable ferric complexes is the first requirement for siderophore-mediated iron acquisition.[56] The second requirement is import of the holo-siderophore across the bacterial cell envelope. To investigate the ability of *A. baumannii* to utilize [Fe(Fim)] as an iron source we performed kinetic growth promotion assays in M9 minimal medium supplemented with 2,2′-dipyridyl (DIP). The same strain of *A. baumaunnii* ATCC 17978 used to isolated Fim and Acb was used in the growth promotion studies. We fine-tuned DIP concentrations, as previously described,[20,22,53] to the point where only weak growth is observed unless an iron supplement is added to the medium (Figure 3). As a positive control, we showed that both Acb and [Fe(Acb)$_2$] recover the growth of *A. baumaunnii* ATCC 17978 in a dose-dependent manner (Figure 3a,c; Supplementary Figures 18 and 19). As expected from our previous work,[20] [Fe(Acb)$_2$] stimulated growth at lower concentrations and to a higher final cell density after 48 h at 37 °C compared to Acb. Similarly, both [Fe(Fim)] and Fim promoted *A. baumannii* growth in a time- and dose-dependent manner with [Fe(Fim)] providing faster and more enhanced growth promotion (Figure 3b,d; Supplementary Figures 18 and 19). Clearly, preloading Acb and Fim with iron(III) is beneficial for growth promotion under these growth conditions. Since [Fe(Acb)$_2$] and [Fe(Fim)] were both prepared as pure ferric complexes with removal of all residual iron, the potent growth stimulating effects must be attributed to utilization of the siderophore ferric complexes as an iron source. These results show for the first time that [Fe(Fim)] can serve as a true iron source for *A. baumannii* ATCC 17978 and support the role of the fimsbactins as natural siderophore substrates.[57]

apo-Fim Antagonizes the Growth Promoting Effects of [Fe(Acb)$_2$]. After establishing the individual roles of Fim and Acb as siderophores, we sought to probe the more challenging question of why *A. baumannii* produces multiple siderophores in the first place. More specifically, we thought it was curious that all pathogenic *A. baumannii* maintain the ability to produce and utilize PreAcb/Acb while <10% produce Fim. We hypothesized that siderophore competition, as opposed to cooperativity, might have led to evolutionary selection of PreAcb/Acb over Fim. To test for siderophore competition between Acb and Fim, we performed checkerboard kinetic growth promotion assays using combinations of Acb, Fim, [Fe(Acb)$_2$], and [Fe(Fim)] against *A. baumannii* ATCC 17978 under the same iron restrictive growth conditions described previously (Figure 4; Supplementary

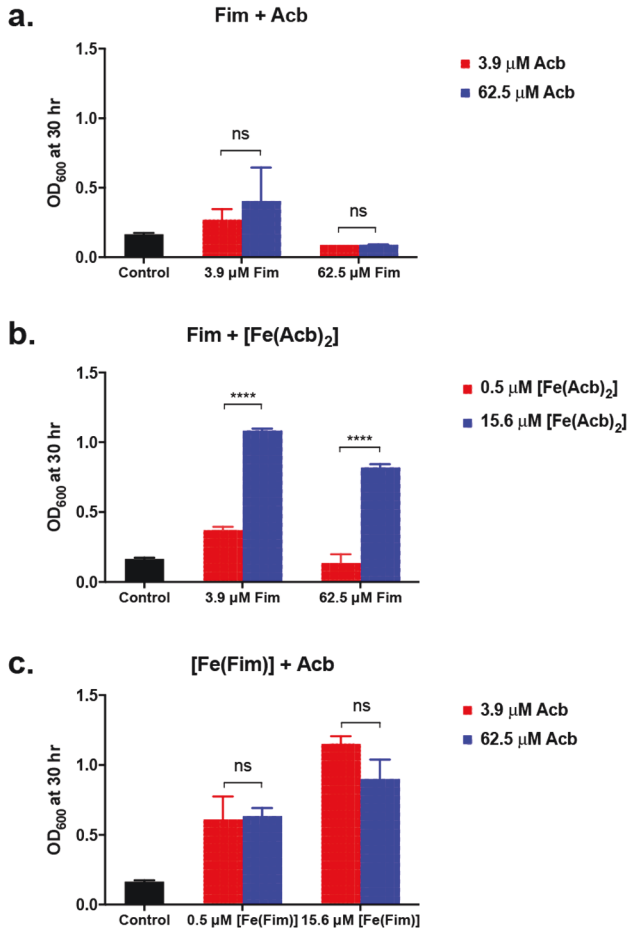

Figure 4. Influence of apo- and holo-siderophore combinations on *A. baumannii* growth. Bar graphs depict the comparison of *A. baumannii* ATCC 17978 growth measured by optical density at 600 nm (OD_{600}) values after 30 h at 37 °C in the presence of variable concentrations of (a) Fim and Acb, (b) Fim and [Fe(Acb)$_2$], and (c) [Fe(Fim)] and Acb. Error bars represent standard deviations from the mean for two independent trials; ****p < 0.0001; ns = not significant.

Figure 20). We were surprised to discover that combinations of apo-siderophores Acb and Fim were growth inhibitory (Figure 4a) compared to each apo-siderophore alone (Figure 3). Increasing the concentration of Acb from 3.9 μM to 62.5 μM in the presence of 3.9 μM Fim slightly recovered growth. Increasing the concentration of Fim to 62.5 μM in the

DOI: 10.1021/acschembio.8b01051
ACS Chem. Biol. 2019, 14, 674−687

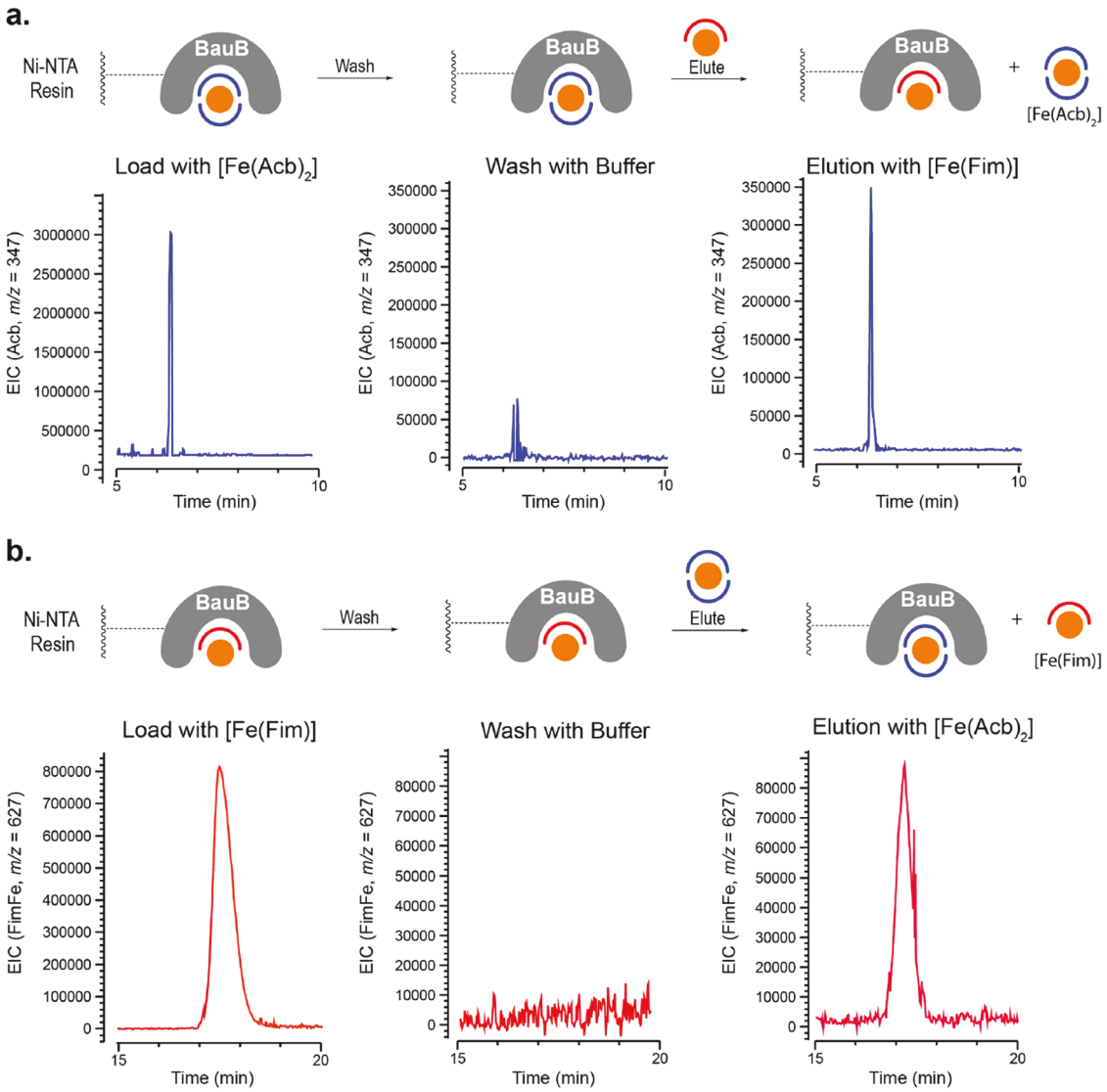

Figure 5. $[Fe(Acb)_2]$ and [Fe(Fim)] compete for BauB binding. *N*-His_6-BauB was immobilized on Ni-NTA resin and loaded with (a) $[Fe(Acb)_2]$ or (b) [Fe(Fim)], washed with phosphate buffer, and eluted with a competing holo-siderophore. Column elutions were analyzed by LC-MS for $[Fe(Acb)_2]$ (m/z = 347) and [Fe(Fim)] (m/z = 627) after each step. Extracted ion chromatograms (EIC) are shown for the initially bound holo-siderophore. EICs are representative for two independent trials.

presence of 62.5 μM Acb returned the antagonistic effect on Acb-promoted growth. The addition of holo-siderophores recovered *A. baumannii* growth but increasing the concentration of apo-siderophores could still antagonize growth slightly. Figure 4b shows that 15.6 μM $[Fe(Acb)_2]$ can recover *A. baumannii* growth in the presence of 3.9 μM or 62.5 μM Fim. However, $[Fe(Acb)_2]$ at 0.5 μM was not capable of recovering growth in the presence of Fim at 3.9 or 62.5 μM. The addition of apo-Acb at 62.5 μM was also slightly antagonistic toward [Fe(Fim)] at 0.5 and 15.6 μM in the growth recovery assay (Figure 4c), although to much lesser extent than the effect of apo-Fim on $[Fe(Acb)_2]$ (Figure 4b). We also investigated the effects of Fim/[Fe(Fim)] combinations on *A. baumannii* growth and discovered slightly reduced growth promotion with increasing concentrations of apo-Fim (Supplementary Figure 21).

The discovery that Fim and Acb appear to be antagonistic adds to the complexity of understanding the delicate balance of metals and siderophores in pathogenic *A. baumannii*. This phenomenon is consistent with our hypothesis that Acb and Fim competition drove natural selection of the Acb pathway found in all *A. baumannii* clinical isolates. In natural environments siderophore competition plays a critical role in microbial population dynamics.[32,42] Siderophore producers often produce siderophore cocktails and express siderophore transport and utilization proteins for xenosiderophores in order to gain a competitive advantage.[32] Some siderophores are inhibitory toward competing bacteria by withholding metals from the extracellular or intracellular environment.[36] Some siderophores are attached to antibiotics, so-called sideromycins, to deliver a toxic payload into susceptible competitor cells.[58] Some siderophores are thought to directly compete for uptake at the receptor level through endogenous pathways.[37,53] Thus, we turned our attention to probing for pathway competition between Acb and Fim in *A. baumannii* to gain further insight into the cause of the antagonistic siderophore relationship.

DOI: 10.1021/acschembio.8b01051
ACS Chem. Biol. 2019, 14, 674−687

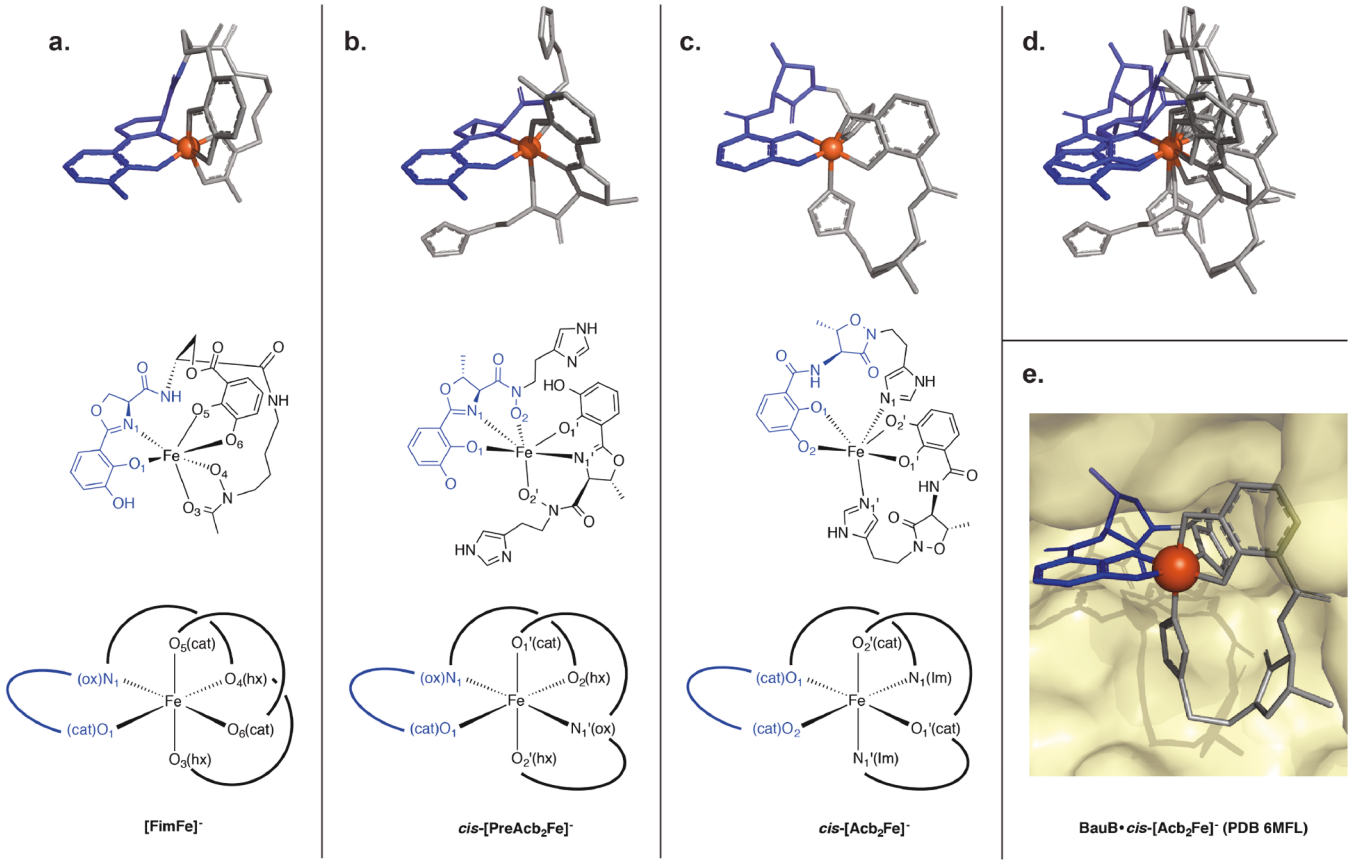

Figure 6. Structural comparison of $[Fe(PreAcb)_2]^-$, $[Fe(Acb)_2]^-$, and $[Fe(Fim)]^-$ complexes. DFT calculated structures of the monoanionic (a) 1:1 $[Fe(Fim)]^-$ and (b) 2:1 *cis*-$[Fe(PreAcb)_2]^-$ complexes (see Experimental Methods for DFT parameters). (c) Experimentally observed structure of the monoanionic *cis*-$[Fe(Acb)_2]^-$ complex bound to the siderophore-binding protein BauB (PDB 6MFL). (d) Overlay of all three structures highlighting similarity of geometry and placement of ligands (ox, oxazoline; cat, catecholate; hx, hydroxamate; im, imidazole) around the ferric iron center. (e) Surface view of the siderophore-binding pocket of BauB occupied by *cis*-$[Fe(Acb)_2]^-$ (PDB 6MFL).

Fim, PreAcb, and Acb Binding to BauB. Bioinformatic analysis of the fimsbactin biosynthetic operon revealed some potential gaps in the uptake pathway, including no dedicated periplasmic siderophore-binding protein (SBP) and no inner membrane permease (Supplementary Figure 3). Outer membrane receptors (OMRs) are often highly selective for binding cognate substrates, while SBPs can be more promiscuous in terms of binding small molecules.[33,56,59] Thus, we hypothesized that the SBP responsible for binding PreAcb/Acb might also bind Fim, which shares structural homology to PreAcb/Acb through the phenolate oxazoline and catecholate moieties. We turned our focus toward BauB, the highly conserved periplasmic SBP responsible for binding PreAcb/Acb and shuttling the corresponding holo-siderophores to the membrane permease, BauCDE, to facilitate import to the cytoplasm. We hypothesized that Fim might compete with PreAcb/Acb for BauB binding and inhibit the import of ferric siderophore complexes to the cytoplasm. To test this hypothesis, we pursued *in vitro* reconstitution of BauB and evaluated the ability of apo- and holo-forms of PreAcb, Acb, and Fim to compete for binding.

We confirmed binding of recombinant BauB to authentic PreAcb and Acb using an intrinsic tryptophan fluorescence quenching assay.[21] We observed dose-dependent fluorescence quenching for both the apo- and holo-forms of both acinetobactin isomers. The binding of both apo- and holo-siderophores by outer membrane siderophore receptors and periplasmic siderophore-binding proteins is common.[33,60] The apparent K_d values for apo-PreAcb and $[Fe(PreAcb)_2]$ were 380 ± 110 nM and 750 ± 160 nM, respectively (Table 1; Supplementary Figure 22).[21] The apparent K_d values for apo-Acb and $[Fe(Acb)_2]$ were 300 ± 100 nM and 160 ± 80 nM, respectively (Table 1).[21] The apparent trend in binding affinities of apo-K_d > holo-K_d for Acb appear to be reversed for the measurements obtained for PreAcb where apo-K_d < holo-K_d. Treatment of BauB with apo- and holo-forms of Fim resulted in dose dependent fluorescence quenching with apparent K_d values falling within the margin of error for those observed for Acb (Table 1). The apparent K_d values for apo-Fim and $[Fe(Fim)]$ were 360 ± 140 nM and 240 ± 90 nM, respectively. All apparent K_d values were calculated using a one-site binding model to fit the binding stoichiometry observed in the BauB·$[Fe(Acb)_2]$ crystal structure.[21] These results are consistent with our hypothesis that PreAcb, Acb, and Fim bind to BauB. We next turned to investigating the reversibility and competitiveness of BauB binding using a siderophore displacement assay with resin-immobilized BauB.

Fimsbactin A and Acinetobactin Directly Compete for Binding to BauB. To validate that Fim binding to BauB is authentic, we performed a competitive binding experiment with $[Fe(Acb)_2]$ and $[Fe(Fim)]$ using resin-immobilized BauB. Our group has reported this type of binding assay previously in the study of ferrioxamine siderophore competition for binding FhuD2, the xenosiderophore receptor displayed on the cell

DOI: 10.1021/acschembio.8b01051
ACS Chem. Biol. 2019, 14, 674−687

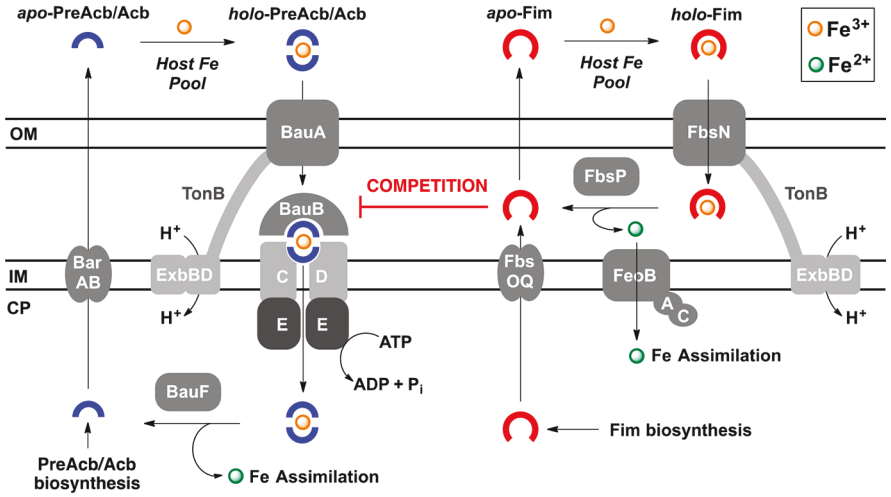

Figure 7. Schematic overview of the PreAcb/Acb and Fim iron acquisition pathways in *A. baumannii*. The Fim pathway has not been experimentally characterized and is hypothesized based on homology to related pathways in Gram-negative bacteria. Periplasmic BauB is highlighted to show interactions with both PreAcb/Acb and Fim connecting the two pathways through competition for the siderophore-binding protein.

surface of pathogenic *Staphylococcus aureus*.[61] *N*-His_6-tagged BauB was adhered to a column of Ni-NTA resin. Saturation of the resin and the quantity of immobilized BauB was determined by SDS-PAGE analysis of column flow through from the protein-loading step. Treatment of the BauB resin with a solution of $[Fe(Acb)_2]$ resulted in a decrease of ion counts in the EIC trace for m/z 347, corresponding to the $[M + H]^+$ ion for Acb (this is the dominant ion in the ESI-MS spectrum of $[Fe(Acb)_2]$[20]). Treatment of the BauB·$[Fe(Acb)_2]$ resin with a solution of [Fe(Fim)] recovered ion counts corresponding to $[Fe(Acb)_2]$, indicating that the excess [Fe(Fim)] displaced $[Fe(Acb)_2]$ to produce the resin bound BauB·[Fe(Fim)] complex with elution of $[Fe(Acb)_2]$ (Figure 5a). Similarly, treatment of the BauB resin with [Fe(Fim)] resulted in a decrease of ion counts in the EIC trace for m/z 627, corresponding to the $[M + H]^+$ ion for [Fe(Fim)] (this is the dominant ion in the ESI-MS spectrum of FimFe) after washing the column with buffer. Treatment of the BauB·[Fe(Fim)] resin with a solution of $[Fe(Acb)_2]$ recovered ion counts for [Fe(Fim)] in the elution, indicating that the excess $[Fe(Acb)_2]$ displaced [Fe(Fim)] from the resin resulting in resin bound BauB·$[Fe(Acb)_2]$ with elution of [Fe(Fim)] (Figure 5b).

We found that the BauB resin could be cycled between treatment with $[Fe(Acb)_2]$ and [Fe(Fim)] multiple times with reversible siderophore displacement. Unfortunately, these competition studies are limited to the use of holo-siderophores since apo-siderophores will bind directly to the Ni-NTA resin.[61] These competition experiments validate that BauB binds tightly and reversible to both $[Fe(Acb)_2]$ and [Fe(Fim)]. Since BauB binding is reversible, the delicate balance between concentrations of apo-siderophores PreAcb, Acb, Fim, and corresponding holo ferric complexes will ultimately determine which siderophore species dominates the BauB binding equilibrium. Our results here show that Fim antagonizes *A. baumannii* growth promotion by $[Fe(Acb)_2]$, suggesting that occupancy of BauB in the periplasm by high concentrations of Fim might exclude utilization of $[Fe(Acb)_2]$ as an iron source. This suggests that the local concentrations of Acb and Fim in the cytoplasm, periplasm, and extracellular space are regulated to minimize pathway competition and optimize iron scavenging under infection conditions.

Structural Similarity of [Fe(Fim)], $[Fe(PreAcb)_2]$, and $[Fe(Acb)_2]$ Ferric Complexes. Accomodation in the BauB substrate binding site requires similarity in the molecular volume, stereochemistry, and geometrical orientation of ligands around the ferric iron center for $[Fe(PreAcb)_2]$, $[Fe(Acb)_2]$, and [Fe(Fim)]. We investigated these properties using density functional theory (DFT) calculations to create energy minimized structural models of $[Fe(PreAcb)_2]^-$ and $[Fe(Fim)]^-$ using the experimentally observed geometry of the $[Fe(Acb)_2]^-$ monoanion in the BauB·$[Fe(Acb)_2]^-$ crystal structure (Figure 6).[21] We assumed that $[Fe(PreAcb)_2]^-$, $[Fe(Acb)_2]^-$, and $[Fe(Fim)]^-$ exist as the mono anions in the ferric complexes. BauB appears to recognize one enantiomer of the *cis*-$[Fe(Acb)_2]^-$ isomeric form. The DFT-computed energy minimized structures of $[Fe(Fim)]^-$ (Figure 6a) and *cis*-$[Fe(PreAcb)_2]^-$ (Figure 6b) were strikingly similar to the experimentally observed *cis*-$[Fe(Acb)_2]^-$ complexed to BauB (Figure 6c). An overlay of the three structures revealed how the common phenolate oxazoline fragment aligns nicely and the L-Ser stereochemistry enables $[Fe(Fim)]^-$ to map the hydroxamate and catecholate ligands to the same ferric binding sites as the imidazole and catecholate ligands of *cis*-$[Fe(Acb)_2]^-$, respectively. As shown in Figure 6e, BauB binds one-half of the *cis*-$[Fe(Acb)_2]^-$ complex through hydrophobic interactions with one of the Acb ligands, while the second Acb ligand remains largely solvent exposed. The computed structures of *cis*-$[Fe(PreAcb)_2]^-$ and $[Fe(Fim)]^-$ would appear to fit this same binding mode to BauB and might explain how all three siderophores can compete for binding to periplasmic BauB. Since [Fe(Fim)] is the only stable 1:1 complex, this could indicate that BauB cannot facilitate transport of 1:1 siderophore/iron complexes across the inner membrane through the associated membrane permease BauCDE hinting at a potential shuttling mechanism for 2:1 PreAcb/Acb−iron complexes (discussed below in more detail).[54,62,63]

A New Model for Siderophore Competition in *A. baumannii*. Our findings are largely consistent with the current understanding of PreAcb/Acb biosynthesis and

DOI: 10.1021/acschembio.8b01051
ACS Chem. Biol. 2019, 14, 674−687

utilization in pathogenic *A. baumannii* (Figure 7). PreAcb is the kinetic biosynthetic product, while Acb is formed via nonenzymatic isomerization of PreAcb as the thermodynamic biosynthetic end product.[18,19] Both PreAcb and Acb can reach the extracellular space, presumably via efflux mediated in part by BarAB.[20] The TonB-dependent OMR BauA has been shown to be essential for PreAcb/Acb utilization, presumably providing import of holo-siderophores to the periplasm.[64,65] The periplasmic SBP BauB, which might be membrane anchored, although this has not been experimentally confirmed,[21] is then thought to shuttle holo-siderophores to the ABC-type membrane permease $BauCDE_2$ where import to the cytoplasm is driven by ATP hydrolysis. BauF is a putative flavin-dependent oxidoreductase responsible for reduction of the ferric holo-siderophore complexes to release ferrous iron for incorporation into protein scaffolds such as the iron−sulfur cluster generating protein SufU.[66] The apo-siderophores, PreAcb or Acb, can then reenter the transport cycle.

Our findings provide new insight into the role of PreAcb, Acb, and Fim in overall siderophore-mediated iron acquisition by *A. baumannii*. The Fim biosynthetic operon contains genes encoding for an efflux pump, FbsOQ, a TonB-dependent OMR, FbsN, and a putative reductase, FbsP. The reductase FbsP is predicted to be secreted to the perisplasm due to the presence of an N-terminal signal sequence, similar to the siderophore-interacting periplasmic reductase FpvC in *Pseudomonas aeruginosa*.[67] We propose that Fim is exported in part by FbsOQ after biosynthesis in the cytoplasm. Extracellular [Fe(Fim)] is presumably imported to the periplasm by FbsN where periplasmic reduction by FbsP releases Fim for efflux and ferrous iron for import to the periplasm via the endogenous ferrous transport system FeoABC.[7,8] This transport model is analogous to the well-studied utilization pathway for the siderophore pyoverdine in pathogenic *P. aeruginosa*.[68] Furthermore, *P. aeruginosa* balances the use of multiple siderophores for adaptive iron acquisition during infection where some siderophores stay in the periplasm (pyoverdine) and some enter the cytoplasm (pyochelin).[69] Analogously, *A. baumannii* might utilize Fim as the periplasmic siderophore and PreAcb/Acb as the cytoplasmic siderophore. This model suggests that Fim never makes it to the cytoplasm, which is consistent with the observation that fimsbactin analogs conjugated to antibiotics with periplasmic targets (β-lactams, daptomycin, vancomycin) show potent, iron-dependent growth inhibitory activity against *A. baumannii* while the same siderophores conjugated to antibiotics with cytoplasmic targets (fluoroquinolones) show no antibacterial activity.[70−72] One unique structural feature of fimsbactin A is the presence of an L-Ser-2,3-DHB ester, which resembles a fragment of the L-Ser-2,3-DHB trilactone scaffold of enterobactin.[24] Similar to enterobactin, it is possible that hydrolysis of the L-Ser-2,3-DHB ester in the periplasm may play a role in iron release.[73] The product of fimsbactin A hydrolysis is fimsbactin F, which is the second most concentrated member of the fimsbactin mixture present in *A. baumannii* ATCC 17978 supernatants (Supplementary Figures 2, 5, 6).

If fimsbactins accumulate in the periplasm, this would create a scenario for competition between Fim and PreAcb/Acb to bind BauB that is consistent with our current findings. A buildup of excess Fim in the periplasm could shift the BauB equilibrium toward a complex of BauB and [Fe(Fim)] and inhibit the import of $[Fe(PreAcb)_2]$ and $[Fe(Acb)_2]$ leading to the growth inhibitory effect that we observed for the siderophore combinations. It is also possible that Fim, PreAcb, and Acb compete for iron and form mixed siderophore ferric complexes that act as transport inhibitors. A crystal structure of the *A. baummannii* OMR BauA bound to a mixed [Fe(PreAcb)(Acb)] ferric complex was recently reported.[74] The BauA·[Fe(PreAcb)(Acb)] structure shows complexation of the iron by a PreAcb ligand through phenolate oxazoline, hydroxamate, and imidazole filling four of the size coordination sites in the octahedral ferric center. The final two coordination sites are apparently filled by the 2,3-DHB catecholate of the Acb ligand. The structure suggests that BauA only interacts with the PreAcb ligand while the Acb dangles outside of the binding pocket. Our group recently reported a competitive inhibitor of siderophore uptake based on an oxidized analog of PreAcb that induces an iron-dependent growth inhibitory effect on *A. baumannii* that is similar to the effect of apo-Fim.[53] The oxidized PreAcb features an aromatic oxazole in place of the PreAcb oxazoline that stabilizes the PreAcb structure and prevents isomerization to Acb. The BauA·[Fe(PreAcb)(Acb)] structure suggests that apo- and holo-variants of the oxazole PreAcb or fimsbactin A might also bind to BauA in a similar manner, although this requires experimental validation. One possibility is that PreAcb stays bound to BauA and BauB as a cofactor to facilitate iron trafficking with ligand exchange.[54,62,63]

Our work suggests that competition for periplasmic BauB is possible, but it is not entirely clear whether competition for BauA plays a role in the growth inhibitory effect of apo-Fim. We tested the effect of excess apo-Fim on the growth of *A. baumannii* ATCC 19606T, a strain that does not produce Fim but does produce PreAcb/Acb and is predicted to produce baumannoferrin (Supplementary Figure 23).[12,64] Treatment of wild-type *A. baumannii* ATCC 19606T with apo-Fim under iron-deficient minimal medium conditions weakly promoted growth at low does; an effect that diminishes at higher doses of apo-Fim (Supplementary Figures 24 and 25). Addition of [Fe(Fim)] promoted the growth of *A. baumannii* ATCC 19606T wild-type and mutant variants s1 (insertional mutant in *basD*, deficient in PreAcb/Acb biosynthesis), t6 (insertional mutation in *bauA*, deficient in PreAcb/Acb import to periplasm), and t7 (insertional mutation in *bauD*, deficient in PreAcb/Acb import to cytoplasm) at low doses. This suggests that [Fe(Fim)] can serve as an iron source in the absence of the dedicated Fim utilization proteins FbsOQNP and Fim bioactivity is independent of acinetobactin biosynthesis and the presence of functional BauA/BauD. It is possible that [Fe(Fim)] can be imported through one of the other ∼20 TonB-dependent outer membrane receptors present in pathogenic strains of *A. baumannii*.[15] We hypothesize that periplasmic accumulation of Fim might contribute to inhibition of *A. baumannii* growth promotion by holo-siderophores, including Acb. A recent study in *Mycobacterium tuberculosis* showed that a siderophore efflux mutant accumulated toxic concentrations of mycobactin siderophores supporting the idea that maintaining the appropriate balance of intracellular siderophores is critical to balance metal homeostasis.[75] Regardless of the underlying cause of apo-Fim inhibition of *A. baumannii* growth, pathway competition between PreAcb, Acb, and Fim seems to be important even for nonproducers of the fimsbactins, including the majority of *A. baumannii* clinical isolates.

DOI: 10.1021/acschembio.8b01051
ACS Chem. Biol. 2019, 14, 674−687

CONCLUSIONS

Pathogenic bacteria often produce multiple siderophores to enhance iron acquisition, expand capacity for metal scavenging, evade the human immune system, and gain a competitive edge in mixed microbial environments. All genome sequenced clinical isolates of the MDR Gram-negative pathogen *A. baumannii* produce the siderophores PreAcb, Acb, and baumannoferrin. PreAcb and Acb both enhance iron acquisition and contribute to pathogen virulence, while the role of baumannoferrin has not yet been investigated. A small percentage (<10%) of *A. baumannii* clinical isolates produce a third family of siderophores known as the fimsbactins. We have shown that *A. baumannii* ATCC 17978 produces Acb in greater quantities than Fim and both siderophores can be purified from culture supernatants. Here, we show that fimsbactin A, the primary component of the fimsbactin siderophore mixture, antagonizes *A. baumannii* growth promotion by Acb and [Fe(Acb)$_2$]. The two siderophores compete directly for binding to the periplasmic siderophore-binding protein BauB implying that pathway competition might contribute to the antagonistic effect of Fim. This competition might explain why the majority of *A. baumannii* clinical isolates have lost the ability to produce the fimsbactins, but have maintained genes for Acb biosynthesis and utilization in a highly conserved manner. Due to the structural similarities of Fim, PreAcb, and Acb, sharing common NRPS-derived fragments from phenolate oxazolines and catecholates from 2,3-DHB, we propose that the fimsbactin scaffold serves as an ideal template for designing new siderophore−antibiotic conjugates that can outcompete native siderophores for cell entry under infection conditions, although this antibiotic delivery strategy should be reserved for antibiotics with periplasmic targets since our current understanding of the fimsbactin pathway suggests import is limited to the periplasm.[70−72] The inherent growth inhibitory effect of apo-Fim toward *A. baumannii* also presents the opportunity to design competitive inhibitors of siderophore uptake that might serve as antivirulence agents to starve the pathogen of iron.[36,53] Our findings suggest that regulation of relative siderophore concentrations, perhaps through control of gene transcription,[76] in pathogens that produce multiple siderophores might be important for minimizing competition and enhancing cooperation between the associated iron uptake pathways. Further studies on the effects of natural siderophore combinations are needed to reveal the subtle details of cooperativity and competition at the transcriptional, biochemical, and cellular level of bacterial iron acquisition.

EXPERIMENTAL METHODS

Strains, Materials, and Instrumentation. Growth studies were conducted using *A. baumannii* ATCC 17978, ATCC 19606T. The s1, t6, and t7 mutant strains of *A. baumannii* ATCC 19606T were obtained from Prof. Luis Actis (Miami University).[64] Precultures and 96-well plate *A. baumannii* growth assays were performed in filter-sterilized M9 minimal media. M9 minimal media was prepared for all experiments as previously described.[20,22,53] Samples for LC-MS were prepared in 0.45 μM PTFE mini-UniPrep vials from Agilent. All preparatory HPLC was performed using a Beckman Coulter SYSTEM GOLD 127P solvent module and 168 detector with a Phenomenex Luna 10u C18(2) 100A column, 250 mm × 21.20 mm, 10 μm with guard column. Prep HPLC was performed with a mobile phase of 5 mM ammonium acetate in (A) water and (B) acetonitrile, and data were processed using 32 Karat software, v7.0. LC-MS was performed on an Agilent 6130 quadrupole LC-MS with G1313 autosampler, G1315 diode array detector, and 1200 series solvent module. A Phenomenex Gemini C18 column, 50 mm × 2 mm, 5 μm with guard column was used for all LC-MS separations. LC-MS mobile phases were 0.1% (v/v) formic acid in (A) water and (B) acetonitrile, and data were processed using G2710 ChemStation software. NMR was performed on a Varian Unity Inova-600 MHz instrument with a cold probe. Bacterial growth studies were performed using polystyrene 96-well plates with polystyrene lids. OD_{600} measurements were taken on a Molecular Devices SpectraMax Plus 384 plate reader.

Isolation and Purification of Acb and Fim. PreAcb was synthesized as described previously by our group.[20] Acb and Fim were isolated and purified from *A. baumannii* ATCC 17978 cultures using a modified literature procedure.[16,20] Briefly, 1 L cultures of *A. baumannii* ATCC 17978 were grown overnight in M9 minimal media. Cells were pelleted, and the supernatant was adjusted to pH ≈ 6 using citric acid. XAD-7HP resin was added to the supernatant, and the mixture was shaken gently. The mixture was filtered, and the resin was washed with methanol. The methanol washings were combined and concentrated via rotary evaporation under reduced pressure. Acb (retention time 12 min, 31 mg/L) and Fim (retention time 15 min, 5 mg/L) were purified from the crude residue by preparatory HPLC (gradient of 0% B to 95% B (v/v) over 17 min, then 95% B to 100% B (v/v) over 8 min). Fim represents a mixture of fimsbactin A (>90%) and fimsbactins B, C, and F (≤10%) as judged by NMR and LC-MS analysis (Supplementary Table 1; Supplementary Figures 5, 6, 8−12). Acb was >95% pure as judged by NMR and LC-MS (Supplementary Figure 7). The holo-siderophores were prepared by mixing PreAcb, Acb, and Fim with excess Fe(acac)$_3$ in methanol followed by concentration and trituration with Et_2O to provide the pure [Fe(PreAcb)$_2$], [Fe(Acb)$_2$], and [Fe(Fim)] ferric complexes.[20,22]

Determination of FimFe Complex Stoichiometry. A 300 μL solution of 570 μM Fim in methanol was prepared. A fluorescence emission spectrum was recorded ($\lambda_{excitation}$ = 330 nm; $\lambda_{emission}$ = 380 nm). To determine stoichiometry of the complex between Fim and Fe(III), 1 μL aliquots of a methanolic solution of 10 mM Fe(acac)$_3$ or $FeCl_3$ were added 0.044 equiv at a time via Hamilton syringe, and emission spectra were recorded after each addition. Peak fluorescence (Abs_{380nm}) was plotted against Fe(III) equivalents to reveal a 1:1 final stoichiometry for the [Fe(Fim)] complex (Supplementary Figure 14).

Determination of Apparent K_{Fe} for [Fe(Fim)]. A stock solution of 100 μM [Fe(Fim)] was prepared in 10 mM HEPES buffer (10 mM HEPES, 600 mM NaCl, 100 mM KCl, pH 7.4), and an optical absorbance spectrum was obtained from λ = 300−800 nm (Supplementary Figure 15). While continuously monitoring optical absorbance at 500 nm, EDTA was added at a final concentration of 120 μM (1.2 equiv relative to [Fe(Fim)]). The apparent iron-binding affinity (K_{Fe}) was determined based on the change in optical absorbance at 500 nm after 800 min for two independent trials using the equations provided in the Supporting Information (Supplementary Figure 16).

Iron Exchange between [Fe(Acb)$_2$] and Fim. [Fe(Acb)$_2$], 300 μL of a 100 μM solution in phosphate buffer (50 mM potassium phosphate pH 8.0, 150 mM NaCl, 1 mM DTT, 5% glycerol), was added to a quartz cuvette. The solution was mixed and allowed to stand for 20 min before an optical absorbance spectrum was collected (400−700 nm). One microliter aliquots of apo-Fim were added consecutively to increase the concentration of apo-Fim from 30 to 210 μM in 30 μM increments. After each addition of apo-Fim, the solution was allowed to stand for 20 min at RT before an optical absorbance spectrum was collected (400−700 nm). Once the final concentration of 210 μM apo-Fim was reached, the solution was allowed to stand for 20 h at RT before an optical absorbance spectrum was collected (400−700 nm) (Supplementary Figure 17).

***A. baumannii* Growth Studies.** Stock solutions of Acb, Fim, [Fe(Acb)$_2$], and [Fe(Fim)] were prepared in M9 media at 250 μM (up to 2.5% (v/v) final DMSO). Each well of a 96-well plate was filled with 50 μL of M9 media, and 50 μL of the 250 μM test compound stock solutions was added to the first row of a 96 well plate to provide 100 μL total volume per well. Compounds were serially diluted down the plate to 3.9 μM by removing 50 μL from the first row of wells and

DOI: 10.1021/acschembio.8b01051
ACS Chem. Biol. 2019, 14, 674−687

diluting down the plate, discarding the last 50 μL, to afford 50 μL in each well. An inoculum was made by adding 100 μL of 0.5 McFarland standard (*A. baumannii* ATCC 17978, ATCC 19606T, wt, s1, t6, and t7 mutants) to 4.0 mL of M9 minimal media supplemented with 350 μM 2,2′-dipyridyl (DIP). Inoculum (50 μL) was added to each well resulting in a final volume of 100 μL per well with a final concentration of 175 μM DIP per well and a serial dilution of test compounds ranging from 62.5−1.95 μM. Bacterial growth was monitored at 37 °C by measuring OD_{600} using a microplate reader (Molecular Devices SpectraMax Plus 384 plate reader). Control experiments were performed in M9 media with 175 μM DIP and no test compounds. DIP concentrations were optimized prior to each experiment by serial dilution against *A. baumannii* under the growth conditions described in this section. All experiments were performed in triplicate as independent trials.

Combinations of Acb, Fim, and the corresponding ferric complexes were evaluated for bacterial growth promotion in a similar manner at 37 °C. A 96-well plate was first filled with 40 μL of M9 minimal media per well and 5 μL of each test compound solution. Fifty microliters of the inoculum in M9 media was added to each well giving a final concentration of 175 μM DIP per well and a total volume of 100 μL per well. Compounds were tested in combinations ranging from 0.5−62.5 μM as summarized in Supplementary Table 2. All experiments were performed in duplicate as independent trials.

Determination of Apparent K_d Values for BauB. BauB was expressed as the N-terminal hexahistidine fusion, *N*-His_6-BauB, in *E. coli* BL21 (DE3) as described previously (Supplementary Figure 26).[21] *N*-His_6-BauB was recovered on ice from a −80 °C freezer stock. A 400 nM BauB stock solution was prepared in assay buffer (25 mM Tris-HCl, 8 g/L NaCl, 0.2 g/L KCl, pH 7.4). For each measurement, 300 μL of the BauB stock solution was transferred to a fluorescence cuvette (HellmaAnalytics High Precision Cell cuvette made of quartz SUPRASIL; light path 10 mm × 2 mm) in the presence of substrate (PreAcb, $[Fe(PreAcb)_2]$, Acb, $[Fe(Acb)_2]$, Fim, Fe(Fim)]) at concentrations ranging from 100 to 1200 nM. Emission spectra were recorded at $\lambda_{emission}$ = 300−400 nm using a PerkinElmer LS 55 luminescence spectrometer (slit width 10 nm; scan speed 400 nm/min) at $\lambda_{excitation}$ = 280 nm. Fluorescence intensity at 320 nm was plotted versus substrate concentration (nM), and apparent K_d was calculated using nonlinear regression and a one binding site model in GraphPad Prism v7.0b (Supplementary Figure 22).[21] All experiments were performed in duplicate as independent trials.

Siderophore Competition Studies with Immobilized BauB. *N*-His_6-BauB was immobilized on Ni-NTA resin following a literature protocol for performing siderophore-affinity chromatography.[61] Saturation of the Ni-NTA resin (2.3 cm × 1 cm resin volume) with BauB was confirmed by SDS-PAGE analysis of the column flow through. The Ni-NTA-BauB column was washed thoroughly with phosphate buffer (50 mM potassium phosphate, pH 8.0, 150 mM NaCl, 1 mM BME, 5% glycerol). A solution of $[Fe(Acb)_2]$ (5 mL, 0.1 mg mL^{-1}) was loaded onto the column, and column was rocked gently for 30 min at 4 °C. Column flow through was collected, and the resin was washed with excess phosphate buffer (5 × 5 mL). [Fe(Fim)] (5 mL, 0.1 mg mL^{-1}) was then loaded, and the column was gently rocked for 30 min at 4 °C. The flow through was collected, and the resin was washed with excess phosphate buffer (5 × 5 mL). $[Fe(Acb)_2]$ (5 mL, 0.1 mg mL^{-1}) was then added back onto the column, and after rocking for 30 min, the flow through was collected. Aliquots of the column loading solutions and elutions were analyzed by LC-MS for the presence of $[Fe(Acb)_2]$ and [Fe(Fim)]. For $[Fe(Acb)_2]$, the extracted ion chromatogram (EIC) for m/z = 347, corresponding to the $[M + H]^+$ for apo-Acb, was plotted. For [Fe(Fim)], the EIC for m/z = 627 corresponding to the $[M + H]^+$ for holo-[Fe(Fim)] was plotted.

DFT Calculations. Stable holo-siderophore complexes with ferric iron were calculated using density functional theory (DFT) following a protocol described previously by our group.[21] We used the crystal structure of the monoanionic $[Fe(Acb)_2]^-$ (S = 5/2) ferric complex bound to BauB (PDB 6FML) as starting geometry of the monoanionic $[Fe(PreAcb)_2]^-$ and $[Fe(Fim)]^-$ ferric complexes.[21]

■ ASSOCIATED CONTENT

Supporting Information

The Supporting Information is available free of charge on the ACS Publications website at DOI: 10.1021/acschembio.8b01051.

Supplementary figures, supplementary tables, supplementary equations, high-resolution mass spectra, LC-MS chromatograms, NMR characterization data, optical absorbance spectra, *A. baumannii* growth curves, and BauB fluorescence quenching plots (PDF)

■ AUTHOR INFORMATION

Corresponding Author

*E-mail: wencewicz@wustl.edu.

ORCID

Timothy A. Wencewicz: 0000-0002-5839-6672

Funding

Research was supported by NSF CAREER Award 1654611 to T.A.W.

Notes

The authors declare no competing financial interest.

■ ACKNOWLEDGMENTS

We thank B. Evans at the Proteomics & Mass Spectrometry Facility at the Donald Danforth Plant Science Center, St. Louis, MO for assistance with the acquisition of the QTRAP LC-MS/MS spectra (supported by the National Science Foundation under Grant No. DBI-0521250). We thank J.-S. Taylor (WUSTL, Dept. of Chemistry) for assistance with fluorescence quenching studies. We thank L. Actis (Miami University) for the s1, t6, and t7 mutant strains of *A. baumannii* ATCC 19606T. We thank A. Gulick and D. Bailey (State University of New York at Buffalo) for the pET28a-TEV plasmid used for expression of BauB.

■ ABBREVIATIONS

A, adenylation domain; Acb, apo-acinetobactin; BME, β-mercaptoethanol; cat., catecholate; CP, cytoplasm; DFT, density functional theory; DTT, dithiothreitol; ESI, electrospray ionization; $[Fe(Acb)_2]$, holo-acinetobactin; [Fe(Fim)], holo-fimsbactin; $[Fe(PreAcb)_2]$, holo-preacinetobactin; Fim, apo-fimsbactin; His_6, hexahistidine; HPLC, high-performance liquid chromatography; hx, hydroxamate; IM, inner membrane; im, imidazole; LB, Luria broth; LC-MS, liquid chromatography−mass spectrometry; MWCO, molecular weight cutoff; Ni-NTA, nickel nitrilotriacetic acid agarose; OM, outer membrane; OMR, outer membrane receptor; ox, oxazoline; PAGE, polyacrylamide gel electrophoresis; PDB, protein data bank; PreAcb, apo-preacinetobactin; rpm, rotations per minute; rt, room temperature; SBP, siderophore-binding protein; SDS, sodium dodecyl sulfate

■ REFERENCES

(1) Harding, C. M., Hennon, S. W., and Feldman, M. F. (2017) Uncovering the mechanisms of *Acinetobacter baumannii* virulence. *Nat. Rev. Microbiol. 16*, 91−102.

(2) Lee, C.-R., Lee, J. H., Park, M., Park, K. S., Bae, I. K., Kim, Y. B., Cha, C.-J., Jeong, B. C., and Lee, S. H. (2017) Biology of Acinetobacter baumannii: Pathogenesis, antibiotic resistance mechanisms, and prospective treatment options. *Front. Cell. Infect. Microbiol. 7*, 55.

DOI: 10.1021/acschembio.8b01051
ACS Chem. Biol. 2019, 14, 674−687

(3) Dickey, S. W., Cheung, G. Y. C., and Otto, M. (2017) Different drugs for bad bugs: antivirulence strategies in the age of antibiotic resistance. *Nat. Rev. Drug Discovery 16*, 457−471.
(4) Gehrke, S. S., Kumar, G., Yokubynas, N. A., Cote, J. P., Wang, W., French, S., MacNair, C. R., Wright, G. D., and Brown, E. D. (2017) Exploiting the sensitivity of nutrient transporter deletion strains in discovery of natural product antimetabolites. *ACS Infect. Dis. 3*, 955−965.
(5) Turner, K. H., Wessel, A. K., Palmer, G. C., Murray, J. L., and Whiteley, M. (2015) Essential genome of *Pseudomonas aeruginosa* in cystic fibrosis sputum. *Proc. Natl. Acad. Sci. U. S. A. 112*, 4110−4115.
(6) Kim, A., Kutschke, A., Ehmann, D. E., Patey, S. A., Crandon, J. L., Gorseth, E., Miller, A. A., McLaughlin, R. E., Blinn, C. M., Chen, A., Nayar, A. S., Dangel, B., Tsai, A. S., Rooney, M. T., Murphy-Benenato, K. E., Eakin, A. E., and Nicolau, D. P. (2015) Pharmacodynamic profiling of a siderophore-conjugated monocarbam in *Pseudomonas aeruginosa*Assessing the risk for resistance and attenuated efficacy. *Antimicrob. Agents Chemother. 59*, 7743−7752.
(7) Álvarez-Fraga, L., Vázquez-Ucha, J. C., Martínez-Guitián, M., Vallejo, J. A., Bou, G., Beceiro, A., and Poza, M. (2018) Pneumonia infection in mice reveals the involvement of the *feoA* gene in the pathogenesis of *Acinetobacter baumannii*. *Virulence 9*, 496−509.
(8) Lau, C. K., Krewulak, K. D., and Vogel, H. J. (2016) Bacterial ferrous iron transport: the Feo system. *FEMS Microbiol. Rev. 40*, 273−298.
(9) Runyen-Janecky, L. J. (2013) Role and regulation of heme iron acquisition in gram-negative pathogens. *Front. Cell. Infect. Microbiol. 3*, 55.
(10) Mihara, K., Tanabe, T., Yamakawa, Y., Funahashi, T., Nakao, H., Narimatsu, S., and Yamamoto, S. (2004) Identification and transcriptional organization of a gene cluster involved in biosynthesis and transport of acinetobactin, a siderophore produced by *Acinetobacter baumannii* ATCC 19606T. *Microbiology 150*, 2587−2597.
(11) Proschak, A., Lubuta, P., Grun, P., Lohr, F., Wilharm, G., De Berardinis, V., and Bode, H. B. (2013) Structure and biosynthesis of fimsbactins A−F, siderophores from *Acinetobacter baumannii* and *Acinetobacter baylyi*. *ChemBioChem 14*, 633−638.
(12) Penwell, W. F., DeGrace, N., Tentarelli, S., Gauthier, L., Gilbert, C. M., Arivett, B. A., Miller, A. A., Durand-Reville, T. F., Joubran, C., and Actis, L. A. (2015) Discovery and characterization of new hydroxamate siderophores, baumannoferrin A and B, produced by *Acinetobacter baumannii*. *ChemBioChem 16*, 1896−1904.
(13) Funahashi, T., Tanabe, T., Mihara, K., Miyamoto, K., Tsujibo, H., and Yamamoto, S. (2012) Identification and characterization of an outer membrane receptor gene in *Acinetobacter baumannii* required for utilization of desferricoprogen, rhodotorulic acid, and desferrioxamine B as xenosiderophores. *Biol. Pharm. Bull. 35*, 753−760.
(14) Moynié, L., Luscher, A., Rolo, D., Pletzer, D., Tortajada, A., Weingart, H., Braun, Y., Page, M. G. P., Naismith, J. H., and Köhler, T. (2017) Structure and function of the PiuA and PirA siderophore-drug receptors from *Pseudomonas aeruginosa* and *Acinetobacter baumannii*. *Antimicrob. Agents Chemother. 61*, e02531.
(15) Antunes, L. C., Imperi, F., Towner, K. J., and Visca, P. (2011) Genome-assisted identification of putative iron-utilization genes in *Acinetobacter baumannii* and their distribution among a genotypically diverse collection of clinical isolates. *Res. Microbiol. 162*, 279−284.
(16) Yamamoto, S., Okujo, N., and Sakakibara, Y. (1994) Isolation and structure elucidation of acinetobactin, a novel siderophore from *Acinetobacter baumannii*. *Arch. Microbiol. 162*, 249−254.
(17) Okujo, N., Sakakibara, Y., Yoshida, T., and Yamamoto, S. (1994) Structure of acinetoferrin, a new citrate-based dihydroxamate siderophore from *Acinetobacter haemolyticus*. *BioMetals 7*, 170−176.
(18) Wuest, W. M., Sattely, E. S., and Walsh, C. T. (2009) Three siderophores from one bacterial enzymatic assembly line. *J. Am. Chem. Soc. 131*, 5056−5057.
(19) Sattely, E. S., and Walsh, C. T. (2008) A latent oxazoline electrophile for N-O-C bond formation in pseudomonine biosynthesis. *J. Am. Chem. Soc. 130*, 12282−12284.
(20) Shapiro, J. A., and Wencewicz, T. A. (2016) Acinetobactin isomerization enables adaptive iron acquisition in *Acinetobacter baumannii* through pH-triggered siderophore swapping. *ACS Infect. Dis. 2*, 157−168.
(21) Bailey, D. C., Bohac, T. J., Shapiro, J. A., Giblin, D. E., Wencewicz, T. A., and Gulick, A. M. (2018) Crystal structure of the siderophore binding protein BauB bound to an unusual 2:1 complex between acinetobactin and ferric iron. *Biochemistry 57*, 6653−6661.
(22) Shapiro, J. A., and Wencewicz, T. A. (2017) Structure-function studies of acinetobactin analogs. *Metallomics 9*, 463−470.
(23) Wang, H., Fewer, D. P., Holm, L., Rouhiainen, L., and Sivonen, K. (2014) Atlas of nonribosomal peptide and polyketide biosynthetic pathways reveals common occurrence of nonmodular enzymes. *Proc. Natl. Acad. Sci. U. S. A. 111*, 9259−9264.
(24) Johnstone, T. C., and Nolan, E. M. (2017) Determination of the molecular structures of ferric enterobactin and ferric enantioenterobactin using racemic crystallography. *J. Am. Chem. Soc. 139*, 15245−15250.
(25) Griffiths, G. L., Sigel, S. P., Payne, S. M., and Neilands, J. B. (1984) Vibriobactin, a siderophore from *Vibrio cholerae*. *J. Biol. Chem. 259*, 383−385.
(26) Carrano, C. J., Jordan, M., Drechsel, H., Schmid, D. G., and Winkelmann, G. (2001) Heterobactins: A new class of siderophores from *Rhodococcus erythropolis* IGTS8 containing both hydroxamate and catecholate donor groups. *BioMetals 14*, 119−125.
(27) Funahashi, T., Tanabe, T., Maki, J., Miyamoto, K., Tsujibo, H., and Yamamoto, S. (2013) Identification and characterization of a cluster of genes involved in biosynthesis and transport of acinetoferrin, a siderophore produced by *Acinetobacter haemolyticus* ATCC 17906T. *Microbiology 159*, 678−690.
(28) Luo, M., Fadeev, E. A., and Groves, J. T. (2005) Membrane dynamics of the amphiphilic siderophore, acinetoferrin. *J. Am. Chem. Soc. 127*, 1726−1736.
(29) Russo, T. A., Olson, R., Macdonald, U., Metzger, D., Maltese, L. M., Drake, E. J., and Gulick, A. M. (2014) Aerobactin mediates virulence and accounts for increased siderophore production under iron-limiting conditions by hypervirulent (hypermucoviscous) *Klebsiella pneumoniae*. *Infect. Immun. 82*, 2356−2367.
(30) Henderson, J. P., Crowley, J. R., Pinkner, J. S., Walker, J. N., Tsukayama, P., Stamm, W. E., Hooton, T. M., and Hultgren, S. J. (2009) Quantitative metabolomics reveals an epigenetic blueprint for iron acquisition in uropathogenic *Escherichia coli*. *PLoS Pathog. 5*, e1000305.
(31) Zane, H. K., Naka, H., Rosconi, F., Sandy, M., Haygood, M. G., and Butler, A. (2014) Biosynthesis of amphi-enterobactin siderophores by *Vibrio harveyi* BAA-1116: identification of a bifunctional nonribosomal peptide synthetase condensation domain. *J. Am. Chem. Soc. 136*, 5615−5618.
(32) McRose, D. L., Seyedsayamdost, M. R., and Morel, F. M. M. (2018) Multiple siderophores: bug or feature? *JBIC, J. Biol. Inorg. Chem. 23*, 983−993.
(33) Endicott, N. P., Lee, E., and Wencewicz, T. A. (2017) Structural basis for xenosiderophore utilization by the human pathogen *Staphylococcus aureus*. *ACS Infect. Dis. 3*, 542−553.
(34) Johnstone, T. C., and Nolan, E. M. (2015) Beyond iron: non-classical biological functions of bacterial siderophores. *Dalton Trans. 44*, 6320−6339.
(35) Abergel, R. J., Wilson, M. K., Arceneaux, J. E., Hoette, T. M., Strong, R. K., Byers, B. R., and Raymond, K. N. (2006) Anthrax pathogen evades the mammalian immune system through stealth siderophore production. *Proc. Natl. Acad. Sci. U. S. A. 103*, 18499−18503.
(36) Bergeron, R. J., Elliott, G. T., Kline, S. J., Ramphal, R., and St James, L., 3rd. (1983) Bacteriostatic and fungostatic action of catecholamide iron chelators. *Antimicrob. Agents Chemother. 24*, 725−730.
(37) Ohlemacher, S. I., Giblin, D. E., d'Avignon, D. A., Stapleton, A. E., Trautner, B. W., and Henderson, J. P. (2017) Enterobacteria

DOI: 10.1021/acschembio.8b01051
ACS Chem. Biol. 2019, 14, 674−687

secrete an inhibitor of Pseudomonas virulence during clinical bacteriuria. *J. Clin. Invest. 127*, 4018−4030.
(38) Amin, S. A., Green, D. H., Hart, M. C., Küpper, F. C., Sunda, W. G., and Carrano, C. J. (2009) Photolysis of iron−siderophore chelates promotes bacterial−algal mutualism. *Proc. Natl. Acad. Sci. U. S. A. 106*, 17071−17076.
(39) Murugappan, R., Karthikeyan, M., Aravinth, A., and Alamelu, M. (2012) Siderophore-mediated iron uptake promotes yeast-bacterial symbiosis. *Appl. Biochem. Biotechnol. 168*, 2170−2183.
(40) Song, L., Zhang, Y., Chen, W., Gu, T., Zhang, S.-Y., and Ji, Q. (2018) Mechanistic insights into staphylopine-mediated metal acquisition. *Proc. Natl. Acad. Sci. U. S. A. 115*, 3942−3947.
(41) Ghssein, G., Brutesco, C., Ouerdane, L., Fojcik, C., Izaute, A., Wang, S., Hajjar, C., Lobinski, R., Lemaire, D., Richaud, P., Voulhoux, R., Espaillat, A., Cava, F., Pignol, D., Borezee-Durant, E., and Arnoux, P. (2016) Biosynthesis of a broad-spectrum nicotianamine-like metallophore in *Staphylococcus aureus*. *Science 352*, 1105−1109.
(42) McRose, D. L., Baars, O., Seyedsayamdost, M. R., and Morel, F. M. M. (2018) Quorum sensing and iron regulate a two-for-one siderophore gene cluster in *Vibrio harveyi*. *Proc. Natl. Acad. Sci. U. S. A. 115*, 7581−7586.
(43) Koh, E.-I., Robinson, A. E., Bandara, N., Rogers, B. E., and Henderson, J. P. (2017) Copper import in *Escherichia coli* by the yersiniabactin metallophore system. *Nat. Chem. Biol. 13*, 1016−1021.
(44) Chaturvedi, K. S., Hung, C. S., Crowley, J. R., Stapleton, A. E., and Henderson, J. P. (2012) The siderophore yersiniabactin binds copper to protect pathogens during infection. *Nat. Chem. Biol. 8*, 731−736.
(45) Jin, Z., Li, J., Ni, L., Zhang, R., Xia, A., and Jin, F. (2018) Conditional privatization of a public siderophore enables *Pseudomonas aeruginosa* to resist cheater invasion. *Nat. Commun. 9*, No. 1383.
(46) Chaturvedi, K. S., Hung, C. S., Giblin, D. E., Urushidani, S., Austin, A. M., Dinauer, M. C., and Henderson, J. P. (2014) Cupric yersiniabactin is a virulence-associated superoxide dismutase mimic. *ACS Chem. Biol. 9*, 551−561.
(47) Qi, B., and Han, M. (2018) Microbial siderophore enterobactin promotes mitochondrial iron uptake and development of the host via interaction with ATP synthase. *Cell 175*, 571−582.
(48) Song, E., Ramos, S. V., Huang, X., Liu, Y., Botta, A., Sung, H. K., Turnbull, P. C., Wheeler, M. B., Berger, T., Wilson, D. J., Perry, C. G. R., Mak, T. W., and Sweeney, G. (2018) Holo-lipocalin-2−derived siderophores increase mitochondrial ROS and impair oxidative phosphorylation in rat cardiomyocytes. *Proc. Natl. Acad. Sci. U. S. A. 115*, 1576−1581.
(49) Smith, M. G., Gianoulis, T. A., Pukatzki, S., Mekalanos, J. J., Ornston, L. N., Gerstein, M., and Snyder, M. (2007) New insights into *Acinetobacter baumannii* pathogenesis revealed by high-density pyrosequencing and transposon mutagenesis. *Genes Dev. 21*, 601−614.
(50) Bollinger, J. G., Rohan, G., Sadilek, M., and Gelb, M. H. (2013) LC/ESI-MS/MS detection of FAs by charge reversal derivatization with more than four orders of magnitude improvement in sensitivity. *J. Lipid Res. 54*, 3523−3530.
(51) Bergeron, R. J., Singh, S., and Bharti, N. (2011) Synthesis of heterobactins A and B and *Nocardia heterobactin*. *Tetrahedron 67*, 3163−3169.
(52) Bao, G., Clifton, M., Hoette, T. M., Mori, K., Deng, S.-X., Qiu, A., Viltard, M., Williams, D., Paragas, N., Leete, T., Kulkarni, R., Li, X., Lee, B., Kalandadze, A., Ratner, A. J., Pizarro, J. C., Schmidt-Ott, K. M., Landry, D. W., Raymond, K. N., Strong, R. K., and Barasch, J. (2010) Iron traffics in circulation bound to a siderocalin (Ngal)-catechol complex. *Nat. Chem. Biol. 6*, 602−609.
(53) Bohac, T. J., Shapiro, J. A., and Wencewicz, T. A. (2017) Rigid oxazole acinetobactin analog blocks siderophore cycling in *Acinetobacter baumannii*. *ACS Infect. Dis. 3*, 802−806.
(54) Stintzi, A., Barnes, C., Xu, J., and Raymond, K. N. (2000) Microbial iron transport via a siderophore shuttle: A membrane ion transport paradigm. *Proc. Natl. Acad. Sci. U. S. A. 97*, 10691−10696.
(55) McQueen, C. F., and Groves, J. T. (2018) A reevaluation of iron binding by mycobactin J. *JBIC, J. Biol. Inorg. Chem. 23*, 995−1007.
(56) Hider, R. C., and Kong, X. (2010) Chemistry and biology of siderophores. *Nat. Prod. Rep. 27*, 637−657.
(57) Ree, H., Kim, J., Song, W. Y., Lee, J. E., and Kim, H. J. (2015) Total syntheses and evaluation of the siderophore functions of fimsbactin B and its analogs. *Bull. Korean Chem. Sci. 36*, 1520−1523.
(58) Wencewicz, T. A., and Miller, M. J. (2018) Sideromycins as pathogen-targeted antibiotics, in *Antibacterials: Vol. II* (Fisher, J. F., Mobashery, S., and Miller, M. J., Eds.), pp 151−183, Springer, Cham.
(59) Krewulak, K. D., and Vogel, H. J. (2008) Structural biology of bacterial iron uptake. *Biochim. Biophys. Acta, Biomembr. 1778*, 1781−1804.
(60) Hoegy, F., Celia, H., Mislin, G. L., Vincent, M., Gallay, J., and Schalk, I. J. (2005) Binding of iron-free siderophore, a common feature of siderophore outer membrane transporters of *Escherichia coli* and *Pseudomonas aeruginosa*. *J. Biol. Chem. 280*, 20222−20230.
(61) Rivera, G. S. M., Beamish, C. R., and Wencewicz, T. A. (2018) Immobilized FhuD2 siderophore-binding protein enables purification of salmycin sideromycins from *Streptomyces violaceus* DSM 8286. *ACS Infect. Dis. 4*, 845−859.
(62) Fukushima, T., Allred, B. E., Sia, A. K., Nichiporuk, R., Andersen, U. N., and Raymond, K. N. (2013) Gram-positive siderophore-shuttle with iron-exchange from Fe-siderophore to apo-siderophore by *Bacillus cereus* YxeB. *Proc. Natl. Acad. Sci. U. S. A. 110*, 13821−13826.
(63) Fukushima, T., Allred, B. E., and Raymond, K. N. (2014) Direct evidence of iron uptake by the gram-positive siderophore-shuttle mechanism without iron reduction. *ACS Chem. Biol. 9*, 2092−2100.
(64) Dorsey, C. W., Tomaras, A. P., Connerly, P. L., Tolmasky, M. E., Crosa, J. H., and Actis, L. A. (2004) The siderophore-mediated iron acquisition systems of *Acinetobacter baumannii* ATCC 19606 and *Vibrio anguillarum* 775 are structurally and functionally related. *Microbiology 150*, 3657−3667.
(65) Gaddy, J. A., Arivett, B. A., McConnell, M. J., López-Rojas, R., Pachón, J., and Actis, L. A. (2012) Role of acinetobactin-mediated iron acquisition functions in the interaction of *Acinetobacter baumannii* Strain ATCC 19606 with human lung epithelial cells, *Galleria mellonella* caterpillars, and mice. *Infect. Immun. 80*, 1015−1024.
(66) Miethke, M. (2013) Molecular strategies of microbial iron assimilation: from high-affinity complexes to cofactor assembly systems. *Metallomics 5*, 15−28.
(67) Ganne, G., Brillet, K., Basta, B., Roche, B., Hoegy, F., Gasser, V., and Schalk, I. J. (2017) Iron release from the siderophore pyoverdine in *Pseudomonas aeruginosa* involves three new actors: FpvC, FpvG, and FpvH. *ACS Chem. Biol. 12*, 1056−1065.
(68) Schalk, I. J., and Guillon, L. (2013) Pyoverdine biosynthesis and secretion in *Pseudomonas aeruginosa* implications for metal homeostasis. *Environ. Microbiol. 15*, 1661−1673.
(69) Cornelis, P., and Dingemans, J. (2013) *Pseudomonas aeruginosa* adapts its iron uptake strategies in function of the type of infections. *Front. Cell. Infect. Microbiol. 3*, 75.
(70) Wencewicz, T. A., and Miller, M. J. (2013) Biscatecholate-monohydroxamate mixed ligand siderophore-carbacephalosporin conjugates are selective sideromycin antibiotics that target *Acinetobacter baumannii*. *J. Med. Chem. 56*, 4044−4052.
(71) Ghosh, M., Lin, Y. M., Miller, P. A., Mollmann, U., Boggess, W. C., and Miller, M. J. (2018) Siderophore conjugates of daptomycin are potent inhibitors of carbapenem resistant strains of *Acinetobacter baumannii*. *ACS Infect. Dis. 4*, 1529−1535.
(72) Ghosh, M., Miller, P. A., Mollmann, U., Claypool, W. D., Schroeder, V. A., Wolter, W. R., Suckow, M., Yu, H., Li, S., Huang, W., Zajicek, J., and Miller, M. J. (2017) Targeted antibiotic delivery: Selective siderophore conjugation with daptomycin confers potent activity against multidrug resistant *Acinetobacter baumannii* both in vitro and in vivo. *J. Med. Chem. 60*, 4577−4583.

DOI: 10.1021/acschembio.8b01051
ACS Chem. Biol. 2019, 14, 674−687

(73) Perraud, Q., Moynie, L., Gasser, V., Munier, M., Godet, J., Hoegy, F., Mely, Y., Mislin, G. L. A., Naismith, J. H., and Schalk, I. J. (2018) A key role for the periplasmic PfeE esterase in iron acquisition via the siderophore enterobactin in *Pseudomonas aeruginosa*. *ACS Chem. Biol. 13*, 2603−2614.
(74) Moeynié, L., Serra, I., Scorciapino, M. A., Oueis, E., Page, M. G., Ceccarelli, M., and Naismith, J. H. (2018) Preacinetobactin not acinetobactin is essential for iron uptake by the BauA transporter of the pathogen *Acinetobacter baumannii*. *eLife 7*, e42270.
(75) Jones, C. M., Wells, R. M., Madduri, A. V. R., Renfrow, M. B., Ratledge, C., Moody, D. B., and Niederweis, M. (2014) Self-poisoning of *Mycobacterium tuberculosis* by interrupting siderophore recycling. *Proc. Natl. Acad. Sci. U. S. A. 111*, 1945−1950.
(76) Gasser, V., Baco, E., Cunrath, O., August, P. S., Perraud, Q., Zill, N., Schleberger, C., Schmidt, A., Paulen, A., Bumann, D., Mislin, G. L. A., and Schalk, I. J. (2016) Catechol siderophores repress the pyochelin pathway and activate the enterobactin pathway in *Pseudomonas aeruginosa* an opportunity for siderophore−antibiotic conjugates development. *Environ. Microbiol. 18*, 819−832.

DOI: 10.1021/acschembio.8b01051
ACS Chem. Biol. 2019, 14, 674−687